Numerical relativity with characteristic evolution, using six angular patches

Christian Reisswig[1], Nigel T. Bishop[2], Chi Wai Lai[2], Jonathan Thornburg[1], and Bela Szilagyi[1]
[1] *Max-Planck-Institut für Gravitationsphysik, Albert-Einstein-Institut, Am Mühlenberg 1, D-14476 Golm, Germany*
[2] *Department of Mathematical Sciences, University of South Africa, P.O. Box 392, Unisa 0003, South Africa*

The characteristic approach to numerical relativity is a useful tool in evolving gravitational systems. In the past this has been implemented using two patches of stereographic angular coordinates. In other applications, a six-patch angular coordinate system has proved effective. Here we investigate the use of a six-patch system in characteristic numerical relativity, by comparing an existing two-patch implementation (using second-order finite differencing throughout) with a new six-patch implementation (using either second- or fourth-order finite differencing for the angular derivatives). We compare these different codes by monitoring the Einstein constraint equations, numerically evaluated independently from the evolution. We find that, compared to the (second-order) two-patch code at equivalent resolutions, the errors of the second-order six-patch code are smaller by a factor of about 2, and the errors of the fourth-order six-patch code are smaller by a factor of nearly 50.

PACS numbers: 04.25.Dm

I. INTRODUCTION

The characteristic, or null-cone, approach to numerical relativity is based on the Bondi-Sachs metric [1, 2], and has been successfully implemented in the PITT code [3, 4, 5, 6, 7, 8] (and also in other codes [9, 10, 11, 12, 13, 14, 15]). The PITT code has the important property that all tests have shown it to be long-term stable, for example in evolving a single black hole spacetime [16]. However, there are problems with the computation of gravitational radiation: it has been successfully computed in test cases [3, 5] and also in scattering problems [17], but it has not been possible to compute gravitational radiation emitted in astrophysically interesting scenarios, such as a star in close orbit around a black hole [7, 18].

This paper is a contribution towards the longer term goal of producing a characteristic code that can reliably compute gravitational radiation in situations of astrophysical interest, either within a stand-alone code [7, 18], or within the context of Cauchy-characteristic extraction or Cauchy-characteristic matching [19]. The first step in this process was to find a class of exact solutions to the linearized Einstein equations [20]. These solutions are written in terms of the Bondi-Sachs metric and continuously emit gravitational radiation. Thus they provide an appropriate testbed for validating further developments of the characteristic code.

In this paper, we investigate a strategy for improving the code. In another context in numerical relativity [21], good results have been obtained by coordinatizing the sphere by means of six angular patches, rather than the two patch stereographic coordinates used in the PITT code. One advantage of the six patch system is that inter-patch interpolation is particularly simple because it is one-dimensional (since ghost zone points lie on grid lines), leading to an expectation of reduced noise at the patch interfaces. Further, this means that it is easy to go from second- to fourth-order accurate finite differencing of angular derivatives, since the interpolation order must also be increased and this is straightforward in the one-dimensional case. Using the exact solutions of ref. [20] as a testbed, we have computed and compared the errors obtained in (a) the stereographic code, (b) the second-order six patch code, and (c) the fourth-order six patch code. Note that, in the fourth-order case, the radial and time derivatives are second-order accurate, so that overall the code is second-order – unfortunately, changing these derivatives to fourth-order would be a major undertaking, because they are not confined to a single subroutine. We found that, for equivalent resolutions, the errors of (b) are a little smaller than those of (a), and that the errors of (c) are much smaller than those of (a) by a factor of nearly 50.

As in the ADM formalism, four of the ten characteristic Einstein equations are not used in the evolution but constitute constraints. We have constructed and validated code that evaluates the constraints, and this can be used as a tool to monitor the reliability of a computational evolution.

The numerical computations presented in this paper were all performed within the Cactus computational toolkit [22] (`http://www.cactuscode.org`), using the Carpet driver [23] (`http://www.carpetcode.org`) to support the multiple-patch computations. The computer algebra results were obtained using Maple.

The plan of the paper is as follows. Sec. II summarizes background material that will be used later. Sec. III describes our implementation of the six patch angular coordinate system. Sec. IV describes the constraint evaluation. Computational results are presented in Sec. V, and are then discussed in the Conclusion, Sec. VI.

II. BACKGROUND MATERIAL

A. The Bondi-Sachs metric

The formalism for the numerical evolution of Einstein's equations, in null cone coordinates, is well known [1, 3, 4, 5, 6, 24]. For the sake of completeness, we give a summary of those aspects of the formalism that will be used here. We start with coordinates based upon a family of outgoing null hypersurfaces. We let u label these hypersurfaces, x^A $(A = 2, 3)$, label the null rays and r be a surface area coordinate. In the resulting $x^\alpha = (u, r, x^A)$ coordinates, the metric takes the Bondi-Sachs form [1, 2]

$$\begin{aligned} ds^2 = &-\left(e^{2\beta}(1 + W_c r) - r^2 h_{AB} U^A U^B\right) du^2 \\ &-2e^{2\beta} du dr - 2r^2 h_{AB} U^B du dx^A + r^2 h_{AB} dx^A dx^B, \end{aligned} \tag{1}$$

where $h^{AB} h_{BC} = \delta^A_C$ and $det(h_{AB}) = det(q_{AB})$, with q_{AB} a metric representing a unit 2-sphere embedded in flat Euclidean 3-space; W_c is a normalised variable used in the code, related to the usual Bondi-Sachs variable V by $V = r + W_c r^2$. As discussed in more detail below, we represent q_{AB} by means of a complex dyad q_A. Then, for an arbitrary Bondi-Sachs metric, h_{AB} can then be represented by its dyad component

$$J = h_{AB} q^A q^B / 2, \tag{2}$$

with the spherically symmetric case characterized by $J = 0$. We also introduce the spin-weighted field

$$U = U^A q_A, \tag{3}$$

as well as the (complex differential) eth operators $\eth$ and $\bar{\eth}$ [25].

Einstein's equations $R_{\alpha\beta} = 8\pi(T_{\alpha\beta} - \frac{1}{2} g_{\alpha\beta} T)$ are classified as: hypersurface equations – $R_{11}, q^A R_{1A}, h^{AB} R_{AB}$ – forming a hierarchical set for β, U and W_c; evolution equation $q^A q^B R_{AB}$ for J; and constraints $R_{0\alpha}$. An evolution problem is normally formulated in the region of spacetime between a timelike or null worldtube and future null infinity, with (free) initial data J given on $u = 0$, and with boundary data for β, U, W_c, J satisfying the constraints given on the inner worldtube.

B. The spin-weighted formalism and the $\eth$ operator

A complex dyad is written

$$q_A = (r_2 e^{i\phi_2}, r_3 e^{i\phi_3}) \tag{4}$$

where r_A, ϕ_A are real quantities (but in general they are not vectors). The real and imaginary parts of q_A are unit vectors that are orthogonal to each other, and q_A represents the metric. Thus

$$q^A q_A = 0, q^A \bar{q}_A = 2, q_{AB} = \frac{1}{2}(q_A \bar{q}_B + \bar{q}_A q_B). \tag{5}$$

It is straightforward to substitute the a 2-metric into Eq. (5) to find r_A and $(\phi_3 - \phi_2)$. Thus q_A is not unique, up to a unitary factor: if q_A represents a given 2-metric, then so does $q'_A = e^{i\alpha} q_A$. Thus, considerations of simplicity are used in deciding the precise form of dyad to represent a particular 2-metric. For example, the dyads commonly used to represent some unit sphere metrics, namely spherical polars and stereographic, are

$$ds^2 = d\theta^2 + \sin^2\theta d\phi^2 : q_A = (1, i\sin\theta); \;\; ds^2 = \frac{4(dq^2 + dp^2)}{(1 + q^2 + p^2)^2} : q_A = \frac{2}{1 + q^2 + p^2}(1, i). \tag{6}$$

Having defined a dyad, we may construct complex quantities representing all manner of tensorial objects, for example $X_1 = T_A q^A$, $X_2 = T^{AB} q_A \bar{q}_B$, $X_3 = T^{AB}_C \bar{q}_A \bar{q}_B \bar{q}^C$. Each object has no free indices, and has associated with it a spin-weight s defined as the number of q factors less the number of $\bar{q}$ factors in its definition. For example, $s(X_1) = 1, s(X_2) = 0, s(X_3) = -3$, and, in general, $s(X) = -s(\bar{X})$. We define derivative operators $\eth$ and $\bar{\eth}$ acting on a quantity V with spin-weight s

$$\eth V = q^A \partial_A V + s\Gamma V, \;\; \bar{\eth} V = \bar{q}^A \partial_A V - s\bar{\Gamma} V \tag{7}$$

where the spin-weights of $\eth V$ and $\bar{\eth} V$ are $s+1$ and $s-1$, respectively, and where

$$\Gamma = -\frac{1}{2} q^A \bar{q}^B \nabla_A q_B. \tag{8}$$

In the case of spherical polars, $\Gamma = -\cot\theta$, and for stereographic coordinates $\Gamma = q + ip$.

The spin-weights of the quantities used in the Bondi-Sachs metric are

$$s(W_c) = s(\beta) = 0,\ s(J) = 2,\ s(\bar{J}) = -2,\ s(U) = 1,\ s(\bar{U}) = -1. \tag{9}$$

We will be using spin-weighted spherical harmonics [26, 27] using the formalism described in [17]. It will prove convenient to use ${}_sZ_{\ell m}$ rather than the usual ${}_sY_{\ell m}$ (the suffix ${}_s$ denotes the spin-weight) as basis functions, where

$$\begin{aligned} {}_sZ_{\ell m} &= \frac{1}{\sqrt{2}}\left[{}_sY_{\ell m} + (-1)^m {}_sY_{\ell -m}\right] \text{ for } m > 0 \\ {}_sZ_{\ell m} &= \frac{i}{\sqrt{2}}\left[(-1)^m {}_sY_{\ell m} - {}_sY_{\ell -m}\right] \text{ for } m < 0 \\ {}_sZ_{\ell 0} &= {}_sY_{\ell 0}, \end{aligned} \tag{10}$$

and note that [17] uses the notation ${}_sR_{\ell m}$ rather than the ${}_sZ_{\ell m}$ used here; we use a different notation to avoid any confusion with the Ricci tensor. In the case $s = 0$, the s will be omitted, i.e. $Z_{\ell m} = {}_0Z_{\ell m}$. Note that the effect of the $\eth$ operator acting on $Z_{\ell m}$ is

$$\eth Z_{\ell m} = \sqrt{\ell(\ell+1)}\ {}_1Z_{\ell m}, \quad \eth^2 Z_{\ell m} = \sqrt{(\ell-1)\ell(\ell+1)(\ell+2)}\ {}_2Z_{\ell m}. \tag{11}$$

C. Linearized solutions

A class of solutions, in Bondi-Sachs form, to the linearized Einstein equations in vacuum was presented in ref. [20], and we use these solutions to test the accuracy of the numerical evolutions described later. More specifically, the solutions to be used are those given in Sec. 4.3 of ref. [20] for the case of a dynamic spacetime on a Minkowski background. We write

$$\begin{aligned} J &= \sqrt{(\ell-1)\ell(\ell+1)(\ell+2)}\ {}_2Z_{\ell m}\Re(J_\ell(r)e^{i\nu u}),\ U = \sqrt{\ell(\ell+1)}\ {}_1Z_{\ell m}\Re(U_\ell(r)e^{i\nu u}), \\ \beta &= Z_{\ell m}\Re(\beta_\ell e^{i\nu u}),\ W_c = Z_{\ell m}\Re(W_{c\ell}(r)e^{i\nu u}), \end{aligned} \tag{12}$$

where $J_\ell(r)$, $U_\ell(r)$, β_ℓ, $W_{c\ell}(r)$ are in general complex, and taking the real part leads to $\cos(\nu u)$ and $\sin(\nu u)$ terms. The quantities β and W_c are real; while J and U are complex due to the terms $\eth^2 Z_{\ell m}$ and $\eth Z_{\ell m}$, representing different terms in the angular part of the metric. We require a solution that is well-behaved at future null infinity, and is well-defined for $r \geq 2$, at which surface we set the inner boundary. We find in the case $\ell = 2$

$$\begin{aligned} \beta_2 &= \beta_0 \\ J_2(r) &= \frac{24\beta_0 + 3i\nu C_1 - i\nu^3 C_2}{36} + \frac{C_1}{4r} - \frac{C_2}{12r^3} \\ U_2(r) &= \frac{-24i\nu\beta_0 + 3\nu^2 C_1 - \nu^4 C_2}{36} + \frac{2\beta_0}{r} + \frac{C_1}{2r^2} + \frac{i\nu C_2}{3r^3} + \frac{C_2}{4r^4} \\ W_{c2}(r) &= \frac{24i\nu\beta_0 - 3\nu^2 C_1 + \nu^4 C_2}{6} + \frac{3i\nu C_1 - 6\beta_0 - i\nu^3 C_2}{3r} - \frac{\nu^2 C_2}{r^2} + \frac{i\nu C_2}{r^3} + \frac{C_2}{2r^4}, \end{aligned} \tag{13}$$

with the (complex) constants β_0, C_1 and C_2 freely specifiable.

We find in the case $\ell = 3$

$$\begin{aligned} \beta_2 &= \beta_0 \\ J_3(r) &= \frac{60\beta_0 + 3i\nu C_1 + \nu^4 C_2}{180} + \frac{C_1}{10r} - \frac{i\nu C_2}{6r^3} - \frac{C_2}{4r^4} \\ U_3(r) &= \frac{-60i\nu\beta_0 + 3\nu^2 C_1 - i\nu^5 C_2}{180} + \frac{2\beta_0}{r} + \frac{C_1}{2r^2} - \frac{2\nu^2 C_2}{3r^3} + \frac{5i\nu C_2}{4r^4} + \frac{C_2}{r^5} \\ W_{c3}(r) &= \frac{60i\nu\beta_0 - 3\nu^2 C_1 + i\nu^5 C_2}{15} + \frac{i\nu C_1 - 2\beta_0 + \nu^4 C_2}{3r} - \frac{i2\nu^3 C_2}{r^2} - \frac{4i\nu^2 C_2}{r^3} + \frac{5\nu C_2}{r^4} + \frac{3C_2}{r^5}. \end{aligned} \tag{14}$$

The emitted gravitational radiation, that is the news N, takes a simple form in the linearized limit when the metric satisfies Eq. (12)

$$N = \Re\left(e^{i\nu u}\lim_{r\to\infty}\left(\frac{\ell(\ell+1)}{4}J_\ell - \frac{i\nu}{2}r^2 J_{\ell,r}\right) + e^{i\nu u}\beta_\ell\right)\sqrt{(\ell-1)\ell(\ell+1)(\ell+2)}\;{}_2Z_{\ell m}. \tag{15}$$

For the cases ℓ =2 and 3,

$$\ell = 2: \quad N = \Re\left(\frac{i\nu^3 C_2}{\sqrt{24}}e^{i\nu u}\right)\;{}_2Z_{2m}; \quad \ell = 3: \quad N = \Re\left(\frac{-\nu^4 C_2}{\sqrt{30}}e^{i\nu u}\right)\;{}_2Z_{3m}. \tag{16}$$

D. Six-patch Angular Coordinates

Given Cartesian coordinates (x, y, z), we define "inflated-cube" angular coordinates on each 2-sphere of constant u and r,

$$\begin{aligned}
\mu &\equiv \text{rotation angle about the } x \text{ axis} = \arctan(y/z)\\
\nu &\equiv \text{rotation angle about the } y \text{ axis} = \arctan(x/z)\\
\phi &\equiv \text{rotation angle about the } z \text{ axis} = \arctan(y/x)
\end{aligned} \tag{17}$$

where all the arctangents are 4-quadrant based on the signs of x, y, and z. We then introduce 6 coordinate patches covering neighborhoods of the $\pm z$, $\pm x$, and $\pm y$ axes, with the angular coordinates $x^A \equiv (\rho, \sigma)$ in each patch defined as follows (see note [29]):

$$(\rho,\sigma) \equiv \begin{cases} (\nu,\mu) & \text{in } \pm z \text{ patches}\\ (\nu,\phi) & \text{in } \pm x \text{ patches}\\ (\mu,\phi) & \text{in } \pm y \text{ patches}\end{cases} \tag{18}$$

Notice that each patch's x^A coordinates are nonsingular throughout a neighborhood of the patch, and that the union of all the patches covers S^2 without coordinate singularities. The name "inflated-cube" comes from another way to visualize these patches and coordinates: Imagine an xyz cube with xyz grid lines painted on its face. Now imagine the cube to be flexible, and inflate it like a balloon, so it becomes spherical in shape. The resulting coordinate lines will closely resemble those for (μ, ν, ϕ) coordinates.

We introduce ghost zones in the usual manner along the angular boundaries of each patch, and we refer to the non-ghost-zone part of each patch's numerical grid as the "nominal" grid. We size the patches so they overlap slightly, with each ghost-zone grid point lying in the nominal grid of some other patch. Figure 1 shows an example of a six-patch system of this type.

We couple the patches together by interpolating the field variables from neighboring patches to each ghost-zone grid point. Notice that with the definition (18), the angular coordinate x^A perpendicular to an interpatch boundary is always common to both the adjacent patches. This means that the interpatch interpolation need only be done in 1 dimension, parallel to the interpatch boundary.

Each patch uses its own $x^A \equiv (\rho, \sigma)$ dyad for the spin-weighted quantities; when interpolating data from one patch to another we transform the data (after interpolation) as described in section III A.

III. IMPLEMENTATION OF SIX PATCH ANGULAR COORDINATES

A. Spin-weighted formalism

The unit sphere metric q_{AB} in each patch is written as

$$ds^2 = \left(1 - \sin^2\rho\,\sin^2\sigma\right)^{-2}\left(\cos^2\sigma\,d\rho^2 + \cos^2\rho\,d\sigma^2 - \frac{1}{2}\sin(2\rho)\sin(2\sigma)\,d\rho\,d\sigma\right), \tag{19}$$

with respect to coordinates (ρ, σ) with range $(-\pi/4, +\pi/4) \times (-\pi/4, +\pi/4)$. A (simple) dyad representing Eq. (19) is

$$q_A = \left(\frac{(\theta_c + i\theta_s)\cos\sigma}{4\theta_c^2\theta_s^2}, \frac{(\theta_c - i\theta_s)\cos\rho}{4\theta_c^2\theta_s^2}\right), \quad q^A = \left(2\theta_c\theta_s\frac{\theta_s + i\theta_c}{\cos\sigma}, 2\theta_c\theta_s\frac{\theta_s - i\theta_c}{\cos\rho}\right), \tag{20}$$

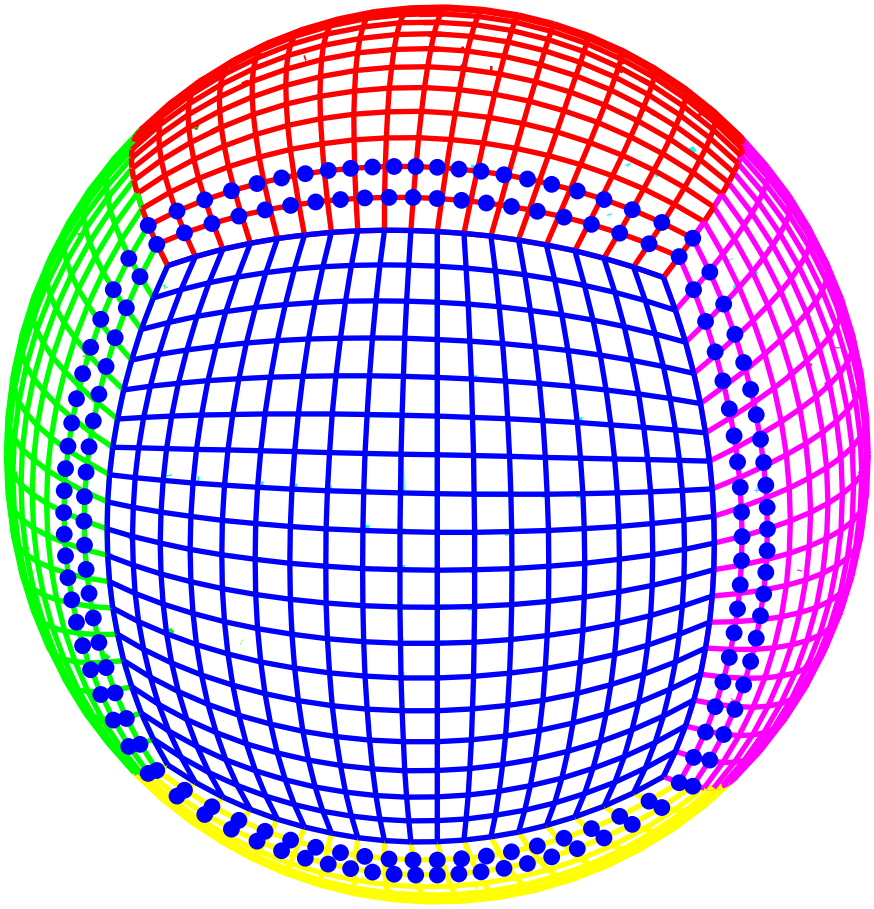

FIG. 1: This figure shows a six-patch grid covering S^2 at an angular resolution of $\Delta x^A = 5^\circ$. Each patch's nominal grid is shown with solid lines; the central patch's ghost-zone points are shown with solid dots. The ghost zone has a width of 2 grid points (suitable for 5-point angular finite difference molecules).

where

$$\theta_c = \sqrt{\frac{1 - \sin\rho \sin\sigma}{2}}, \theta_s = \sqrt{\frac{1 + \sin\rho \sin\sigma}{2}}. \tag{21}$$

The factor Γ, defined in Eq. (8) and needed for the evaluation of $\eth$, works out to be

$$\begin{aligned} \Gamma &= \frac{\cos^2\rho \cos^2\sigma(\sin\rho + \sin\sigma) + (\cos^2\rho - \cos^2\sigma)(\sin\sigma - \sin\rho)}{4\theta_c \cos\sigma \cos\rho} \\ &+ i\frac{\cos^2\rho \cos^2\sigma(\sin\rho - \sin\sigma) + (\cos^2\sigma - \cos^2\rho)(\sin\rho + \sin\sigma)}{4\theta_s \cos\sigma \cos\rho}. \end{aligned} \tag{22}$$

In addition, we need to specify how spin-weighted quantities transform at inter-patch boundaries. Suppose that we have two patches "Old" and "New", with quantities in the two patches being denoted by means of suffices $_{(O)}$ and $_{(N)}$, respectively. Define the Jacobian J^A_B from the old patch to the new patch

$$J^A_B = \frac{\partial x^A_{(N)}}{\partial x^B_{(O)}}. \tag{23}$$

Then the dyad $q^A_{(O)}$ has components in the new coordinates

$$q^A_{(O)[N]} = q^B_{(O)} J^A_B \tag{24}$$

where the notation is that the $_{(O)}$ indicates that we are referring to the dyad that generates the metric in the old patch, and the $_{[N]}$ indicates that the components are given with respect to the new coordinates. Any two complex dyads are related by means of a rotation $\exp(i\gamma)$. Writing

$$q^A_{(N)} = \exp(i\gamma) q^A_{(O)[N]}, \tag{25}$$

and applying Eq. (5), it follows that

$$\exp(i\gamma) = \frac{2}{q_{AB(N)} \bar{q}^A_{(N)} q^B_{(O)[N]}}, \tag{26}$$

and then a spin-weighted quantity V with spin-weight s transforms between the two patches as

$$V_{(N)} = \exp(is\gamma) V_{(O)}. \tag{27}$$

There are many different cases for the transformation between the patches, and we give the transformation and Jacobian explicitly in only one case, when the inter-patch boundary is at

$$\rho_{(O)} = \frac{\pi}{4},\ \rho_{(N)} = -\frac{\pi}{4},\ \sigma_{(O)} = \sigma_{(N)}. \tag{28}$$

Then the coordinate transformation is

$$\rho_{(N)} = \arctan\left(-\frac{1}{\tan\rho_{(O)}}\right),\ \sigma_{(N)} = \arctan\left(\frac{\tan\sigma_{(O)}}{\tan\rho_{(O)}}\right), \tag{29}$$

and the Jacobian evaluates to

$$\frac{\partial\rho_{(N)}}{\partial\rho_{(O)}} = 1,\ \frac{\partial\rho_{(N)}}{\partial\sigma_{(O)}} = 0, \tag{30}$$

$$\frac{\partial\sigma_{(N)}}{\partial\rho_{(O)}} = -\frac{\cos\sigma\sin\sigma}{\cos^2\sigma\sin^2\rho + \cos^2\rho\sin^2\sigma},\ \frac{\partial\sigma_{(N)}}{\partial\sigma_{(O)}} = \frac{\cos\rho\sin\rho}{\cos^2\sigma\sin^2\rho + \cos^2\rho\sin^2\sigma}. \tag{31}$$

B. Computational implementation

The existing stereographic code has been extended to the six patch coordinate system. Since the formulation of the equations in terms of spin-weighted quantities is independent of angular coordinate bases but dyad-dependent, it is necessary to re-implement only those objects that depend on the six patch dyad. We have therefore provided a numerical implementation of the new $\eth$-operators in the code. In addition, we have adapted the spin-transformation coefficients to the six patches. In order to test the six-patch code against the linearized solutions, the spin-weighted spherical harmonics ${}_sZ_{\ell m}$ needed to be implemented for the six-patch coordinates and dyad.

The $\eth$-operators are implemented via subroutines $D_1(s,e)$ and $D_2(s,e_1,e_2)$, which calculate $\eth$ or $\bar{\eth}$ and the second derivative as the combinations $\eth\eth$, $\eth\bar{\eth}$, $\bar{\eth}\eth$ and $\bar{\eth}\bar{\eth}$. The parameter s specifies the spin s of the quantity to which the operator is applied, and $e_1, e_2 \in \{-1, 1\}$ denote $\eth$ and $\bar{\eth}$.

The derivative operators ∂^2_ρ, ∂^2_σ, $\partial_\rho\partial_\sigma$, ∂_ρ and ∂_σ have been approximated by second- and fourth-order accurate centered finite difference stencils [28]. There is an input parameter that enables switching between second- and fourth-order accurate derivatives.

In order to calculate the values of the $\eth$-derivatives at the boundary of each patch, we need to access values from the neighboring patches. This is done by defining ghost zones, which contain the needed values of these patches. The multipatch infrastructure interpolates the spin-weighted (scalar) quantities between the patches using either cubic or quintic Lagrange polynomial interpolation, depending on whether angular derivatives are approximated by second- or fourth-order accurate finite differences. In both cases, the ghost-zone points lie on grid lines, so the interpolation was simple to implement because it was only one dimensional. After the interpolation, we apply the transformation law (27) to transform quantities of spin-weight $s \neq 0$ to the current patch's coordinates and dyad.

It turns out that we need a total number of 12 different spin-transformation coefficients, since we have a $P_\pm$-symmetry between the total number of 24 ghost zones across all P_{+i} and P_{-i}, $i = x, y, z$ patches. These coefficients are calculated and stored for repeated use in an initial routine. After each radial step during the integration of the

characteristic equations, the ghost zones are synchronized by the multipatch infrastructure, and afterwards, the code multiplies the appropriate spin-transformation coefficients with the synchronized values of the ghost zones.

We have carried out checks of the angular grid including the D_1- and D_2-operators and the spin-transformation coefficients, and we have found out that the code converges with second- and fourth-order accuracy, respectively.

The spin-weighted spherical harmonics have been implemented by using the spherical harmonics in terms of the stereographic coordinate $\zeta = p + iq$ and by applying the pseudo-numerical operators D_1 and D_2 in order to obtain ${}_sZ_{\ell m}$ for $|s| > 0$. With pseudo-numerical, we mean that we apply the fourth-order D_1 and D_2 operators with a very small delta-spacing such that we reach machine precision, since we know the $Z_{\ell m}$ everywhere and are not bound to the numerical grid. In order to use the stereographic routines for the $Z_{\ell m}$, we have transformed the stereographic coordinate ζ to the six-patch coordinates and depending on the hemisphere, we use the stereographic routines for north or south patch, respectively.

Furthermore, we have implemented an algorithm for calculating the linearized news function (Eq.(15)), in the form

$$N = \lim_{r\to\infty}\left(\frac{\ell(\ell+1)}{4}J - \frac{1}{2}r^2 J_{,ur} + \eth^2\beta\right). \tag{32}$$

IV. THE CONSTRAINT EQUATIONS

If the boundary data satisfies the constraints $R_{0\alpha} = 0$ (here we restrict attention to the vacuum case), and provided the hypersurface and evolution equations are satisfied, the Bianchi identities guarantee that the constraints are satisfied throughout the domain [1, 2]. Thus from an analytic viewpoint, evaluation of the constraints is redundant, but in a numerical simulation their evaluation may provide useful information concerning the reliability of the computation.

We have written code that uses the Bondi-Sachs metric variables and derivatives to evaluate the following quantities

$$R_{00},\ \ R_{01} \text{ and } q^A R_{0A}. \tag{33}$$

The expressions for the above quantities are very long and are not reproduced here. The Fortran code for these expressions was generated directly from the computer algebra (Maple) output.

V. TESTING THE CODE

In this section we first specify the linearized solutions against which the code will be tested, as well as the various parameters that describe a numerical solution and its output. Then we present, as Figures and Tables, the results of testing the comparative performance of the second order six-patch, fourth order six-patch and stereographic codes.

We refer to the linearized solutions summarized in Sec. II C. In all cases we take

$$\nu = 1 \text{ and } m = 0. \tag{34}$$

We present results for the cases $\ell = 2$ and $\ell = 3$ with

$$C_1 = 3\cdot 10^{-6}, \qquad C_2 = 10^{-6}, \qquad \beta_0 = i\cdot 10^{-6} \qquad (\ell = 2) \tag{35}$$

$$C_1 = 3\cdot 10^{-6}, \qquad C_2 = i\cdot 10^{-6}, \qquad \beta_0 = i\cdot 10^{-6} \qquad (\ell = 3) \tag{36}$$

in Eq. (13) in the case $\ell = 2$, and in Eq. (14) in the case $\ell = 3$.

All the numerical simulations use a compactified radial coordinate $x = r/(r_{wt} + r)$ with $r_{wt} = 9$. Data is prescribed at time $u = 0$ as well as at the inner boundary $r = 2$ (which is equivalent to $x = 0.1888$). The stereographic grids (with ghost zones excluded) are

$$\text{Coarse: } n_x = n_q = n_p = 41, \qquad \text{Fine: } n_x = n_q = n_p = 81; \tag{37}$$

and there is no overlap between the two patches, i.e. we set the code parameter $q_{\text{size}} = 1$ which means that on the nominal grid, the holomorphic coordinate function $\zeta = q + ip$ takes values in $q, p \in [-1, 1]$. The six-patch grids are such that, over the whole sphere, the total number of angular cells is equivalent. We take

$$\text{Coarse: } n_x = 41, \quad n_\sigma = n_\rho = 24, \qquad \text{Fine: } n_x = 81, \quad n_\sigma = n_\rho = 47. \tag{38}$$

TABLE I: Comparative performance in the $\ell = 2$ case

	Stereographic	six-patch, 2nd order	six-patch, 4th order
Averaged convergence rate of J	3.8456	3.8286	3.9112
Averaged absolute error of J	3.3039×10^{-9}	1.5491×10^{-9}	6.9157×10^{-11}
Averaged convergence rate of N	3.3119	3.9642	3.5528
Averaged absolute error of N	2.2785×10^{-8}	1.0913×10^{-8}	8.4414×10^{-10}
Averaged convergence rate of R_{00}	1.2487	1.5000	2.0319
Averaged absolute error of R_{00}	3.1942×10^{-9}	2.8779×10^{-9}	5.7668×10^{-10}
Averaged convergence rate of R_{01}	3.5560	3.5936	3.1296
Averaged absolute error of R_{01}	3.9214×10^{-11}	1.6988×10^{-11}	2.7331×10^{-12}
Averaged convergence rate of R_{0A}	3.4285	1.7558	2.0043
Averaged absolute error of R_{0A}	5.2549×10^{-9}	6.6397×10^{-9}	2.1543×10^{-9}

TABLE II: Comparative performance in the $\ell = 3$ case

	Stereographic	six-patch, 2nd order	six-patch, 4th order
Averaged convergence rate of J	3.9783	3.9106	4.0777
Averaged absolute error of J	4.6461×10^{-9}	3.2784×10^{-9}	1.3677×10^{-10}
Averaged convergence rate of N	2.1201	3.9134	3.6262
Averaged absolute error of N	4.9174×10^{-8}	2.8182×10^{-8}	1.7996×10^{-9}
Averaged convergence rate of R_{00}	1.2743	1.7963	2.0330
Averaged absolute error of R_{00}	7.2594×10^{-9}	4.5824×10^{-9}	1.1744×10^{-9}
Averaged convergence rate of R_{01}	3.5144	3.5383	3.3824
Averaged absolute error of R_{01}	1.3262×10^{-10}	7.5501×10^{-11}	6.0924×10^{-12}
Averaged convergence rate of R_{0A}	3.4326	1.9510	2.0156
Averaged absolute error of R_{0A}	9.0299×10^{-9}	1.0076×10^{-8}	2.9654×10^{-9}

Six-patch results are reported for both second-order and fourth order differencing of the angular derivatives. In all cases, the fine grid has $\Delta u = 0.0125$ and the coarse grid has $\Delta u = 0.025$. Runs are performed for two complete periods, i.e. starting at $u = 0$ and ending at $u = 4\pi$.

Results are reported for the errors of the quantities shown using the L_2 norm, evaluated at the time shown, averaged over all non-ghost grid-points over the whole sphere and between the inner boundary and future null infinity. The norm of the error in the news is averaged over the whole sphere at future null infinity.

The error ϵ for a quantity Ψ is defined as

$$\epsilon(t) = \|\Psi_{numeric} - \Psi_{analytic}\|. \tag{39}$$

The convergence factor C is then defined as the ratio between the error ϵ of low and high resolution

$$C(t) = \frac{\epsilon(t)_{low}}{\epsilon(t)_{high}}. \tag{40}$$

VI. CONCLUSION

We have implemented a version of the characteristic numerical relativity code that coordinatizes the sphere by means of six angular patches. Further, the six-patch code has been implemented for both second-order and fourth-order accurate finite differencing of angular derivatives.

We compared the errors in the second-order six-patch, fourth-order six-patch and stereographic versions of the code, using exact solutions of the linearized Einstein equations as a testbed. This was done for a variety of cases and using several different indicators to measure the error. The convergence rate of the metric (i.e. of J) was always approximately second-order, but in some cases we observed degradation of the order of convergence of other quantities,

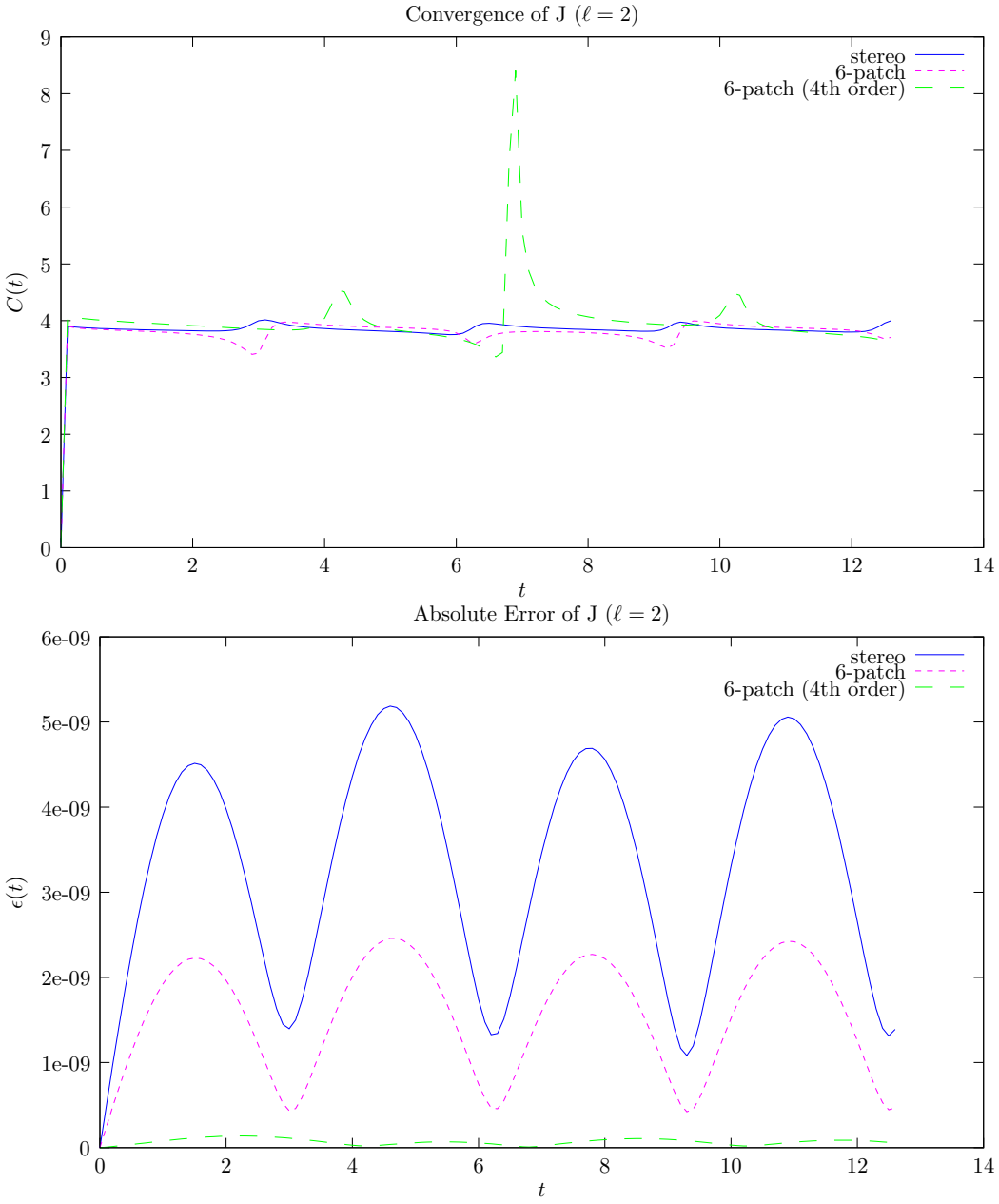

FIG. 2: Convergence factor C and error norm ϵ of J plotted against time in the case $\ell = 2$

all of which contain second derivatives of the metric. This has shown up in previous performed runs of the code and might be related to high-frequency error modes coming from angular patch interfaces or corners. On average, the error norm of second order six-patch was smaller than that of stereographic by a factor of order two (although there were cases in which the error was slightly larger). However, the fourth-order six-patch scheme exhibited a dramatic reduction in the error norm, by a factor of up to 47 compared to that of the stereographic case.

Thus, we expect the six-patch characteristic code, in particular the version that uses fourth-order accurate angular finite differencing, to give significantly better performance than the stereographic version.

Acknowledgments

NTB and CWL thank Max-Planck-Institut für Gravitationsphysik, Albert-Einstein-Institut, for hospitality; and BS and CR thank the University of South Africa for hospitality. The work was supported in part by the National

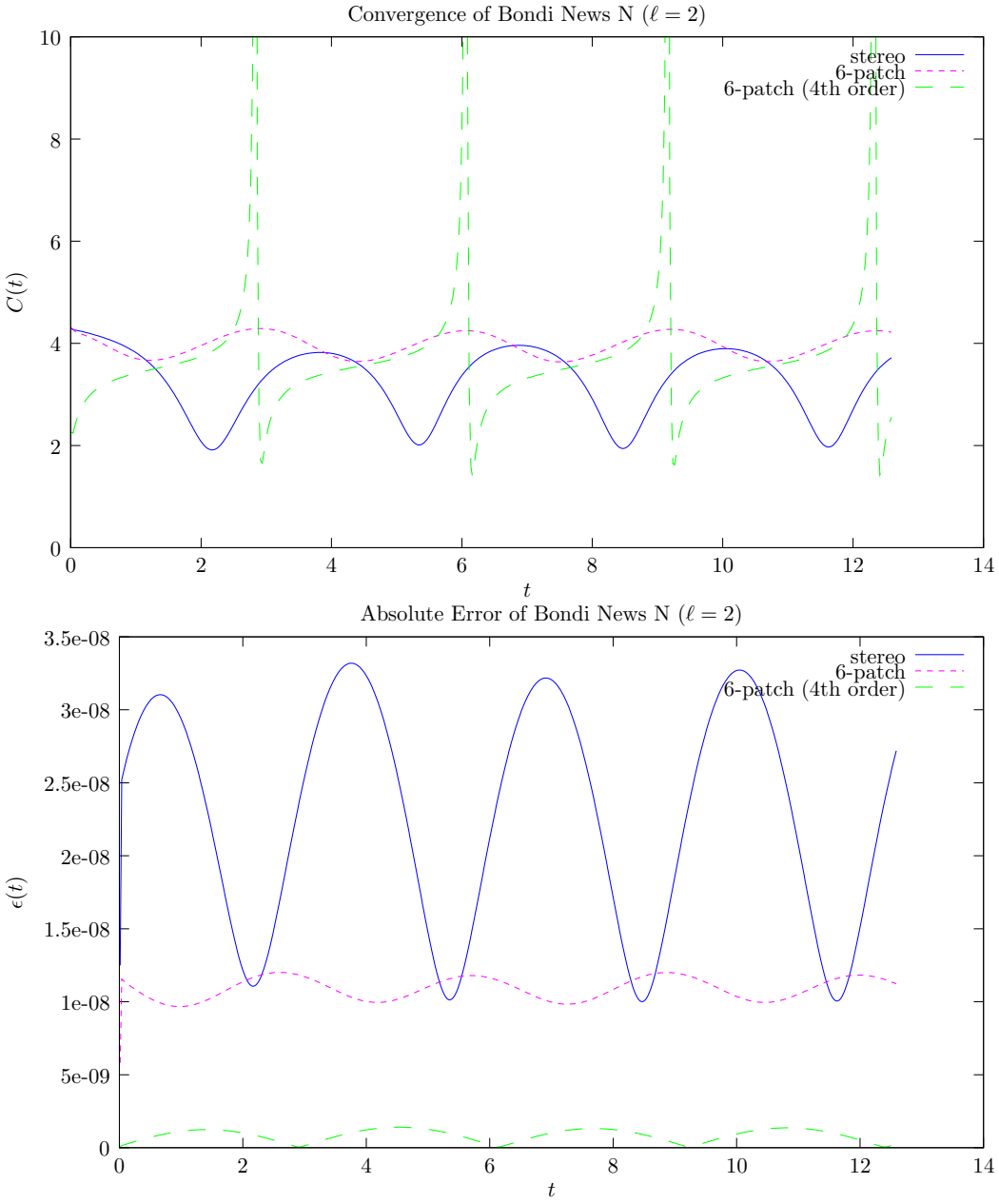

FIG. 3: Convergence factor C and error norm ϵ of N plotted against time in the case $\ell = 2$

Research Foundation, South Africa, under Grant number 2053724.

[1] H. Bondi, M.J.G. van der Burg and A.W.K. Metzner, Proc. R. Soc. **A269**, 21 (1962).
[2] R.K. Sachs, Proc. R. Soc. **A270**, 103 (1962).
[3] N.T. Bishop, R. Gomez, L. Lehner, M. Maharaj and J. Winicour, Phys. Rev. D **56**, 6298 (1997).
[4] R. Gómez, Phys. Rev. D **64**, 024007 (2001).
[5] N.T. Bishop, R. Gomez, L. Lehner and J. Winicour, Phys. Rev. D **54**, 6153 (1996).
[6] N.T. Bishop, R. Gomez, L. Lehner, M. Maharaj and J. Winicour, Phys. Rev. D **60**, 024005 (1999).
[7] N.T. Bishop, R. Gomez, S. Husa, L. Lehner and J. Winicour, Phys. Rev. D **68**, 084015 (2003).
[8] R. Gomez, S. Husa, L. Lehner and J. Winicour, Phys. Rev. D **66**, 064019 (2002).
[9] N.T. Bishop C.J.S. Clarke and R.A. d'Inverno, Class. Quant. Grav. **7**, L23 (1993).

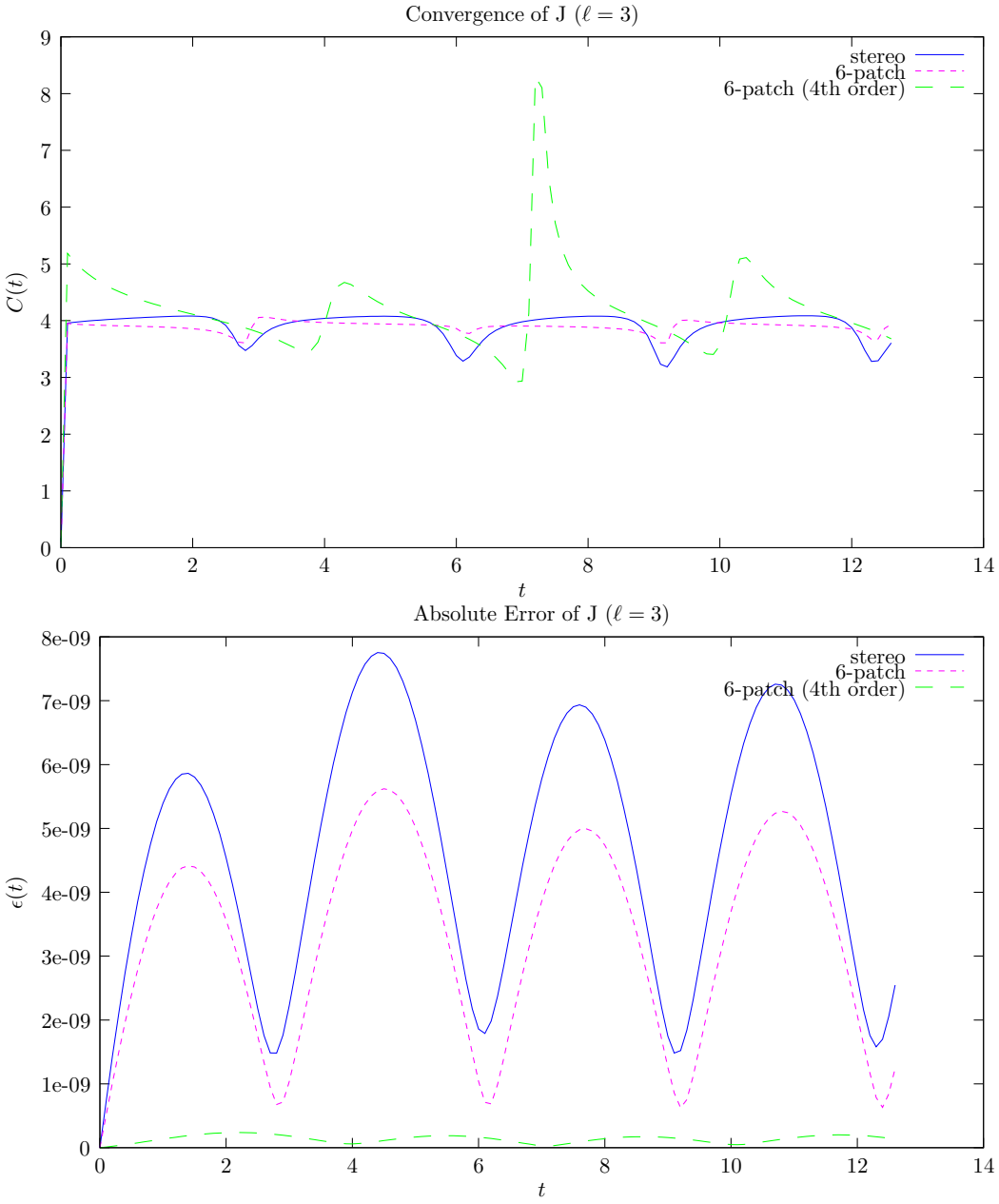

FIG. 4: Convergence factor C and error norm ϵ of J plotted against time in the case $\ell = 3$

[10] R.A. d'Inverno and J.A. Vickers, Phys. Rev. D **56**, 772 (1997).
[11] R.A. d'Inverno, M.R. Dubal and E.A. Sarkies, Class. Quant. Grav. **17**, 3157 (2000).
[12] P. Papadopoulos and J. A. Font, Phys. Rev. D **61**, 024015 (2000).
[13] F. Siebel, J. A. Font, E. Muller and P. Papadopoulos, Phys. Rev. D **67**, 124018 (2003).
[14] F. Siebel, J. A. Font and P. Papadopoulos, Phys. Rev. D **65**, 024021 (2002).
[15] R. Bartnik and A. Norton, http://www.arXiv.org/gr-qc/9904045 (1999).
[16] R. Gomez, L. Lehner, R. L. Marsa and J. Winicour, Phys. Rev. D **57**, 4778 (1998).
[17] Y. Zlochower, R. Gomez, S. Husa, L. Lehner and J. Winicour, Phys. Rev. D **68**, 084014 (2003).
[18] N.T. Bishop, R. Gomez, L. Lehner, M. Maharaj and J. Winicour, Phys. Rev. D **72**, 024002 (2005).
[19] M. Babiuc, B. Szilagyi, I. Hawke and Y. Zlochower, Class. Quantum Grav. **22** 5089-5108 (2005).
[20] N.T. Bishop, Class. Quantum Grav. **22** 2393 (2005).
[21] J. Thornburg, Class. Quantum Grav. **21** 3665-3692 (2004).
[22] T. Goodale, G. Allen, G. Lanfermann, J. Massó, T. Radke, E. Seidel and J. Shalf, Vector and Parallel Processing – VECPAR'2002, 5th International Conference, Springer Lecture Notes in Computer Science.

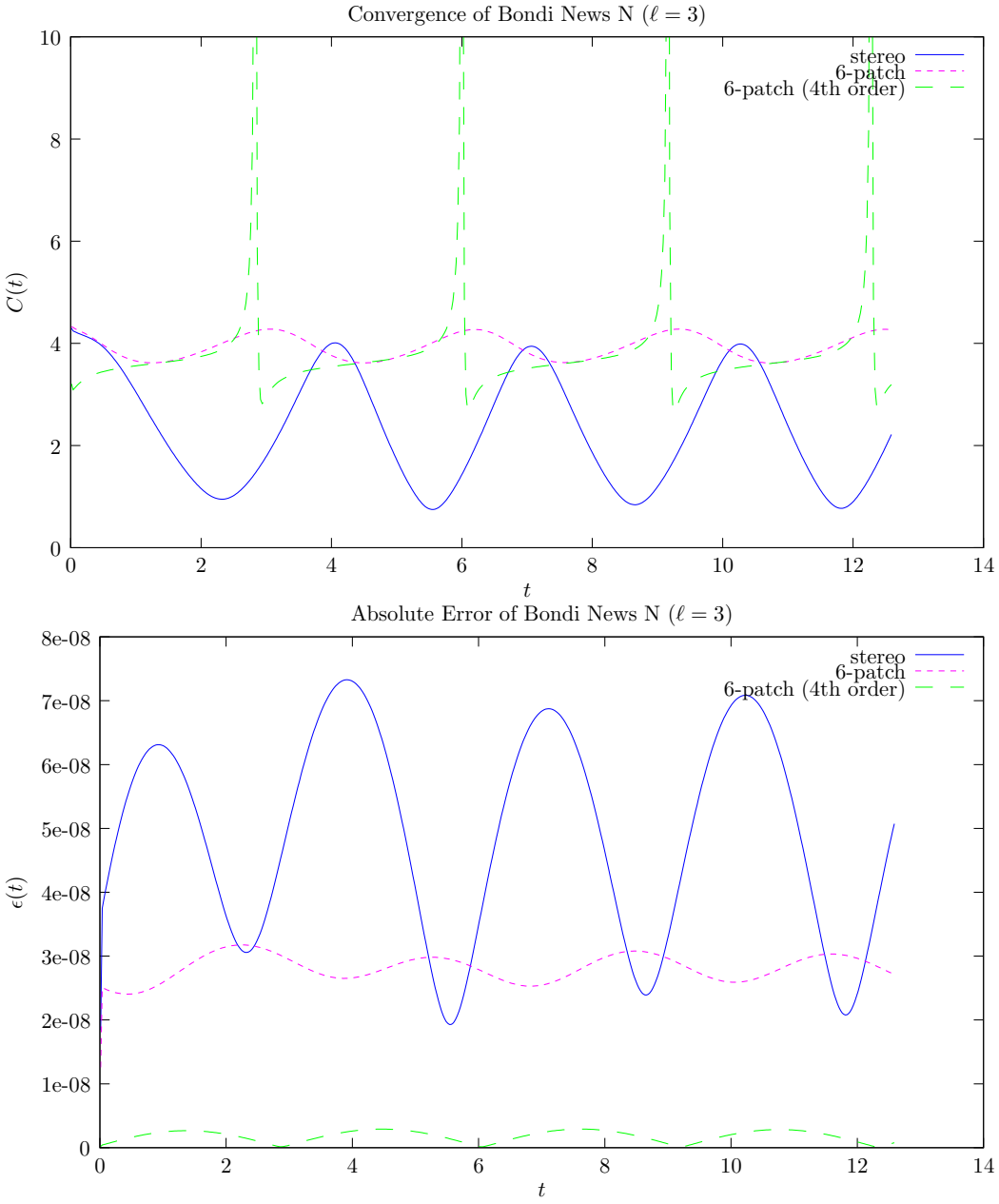

FIG. 5: Convergence factor C and error norm ϵ of N plotted against time in the case $\ell = 3$

[23] E. Schnetter, S. H. Hawley and I. Hawke, Class. Quantum Grav. **21** 1465–1488 (2004).
[24] R.A. Isaacson, J.S. Welling and J. Winicour, Jnl. Math. Phys. **24**, 1824 (1983).
[25] R. Gómez, L. Lehner, P. Papadopoulos and J. Winicour, Class. Quant. Grav. **14**, 977 (1997).
[26] E.T. Newman and R. Penrose, Jnl. Math. Phys. **7**, 863 (1966).
[27] J.N. Goldberg, A.J. MacFarlane, E.T. Newman, F. Rohrlich and E.C.G. Sudarshan, Jnl. Math. Phys. **8**, 2155 (1967).
[28] B. Fornberg, Math. Comp. **51**, 184 (1988)
[29] This definition differs from that of [21] only by the interchange of ρ and σ in $\pm z$ patches. The present definition has the advantage of having a consistent parity, with $\vec{\rho} \times \vec{\sigma}$ always pointing $\{\text{outwards}, \text{inwards}\}$ in $\{+, -\}$ patches.